



CHORUS

This is the accepted manuscript made available via CHORUS. The article has been published as:

Structural coupling across the $\text{LaAlO}_3/\text{SrTiO}_3$ interface: High-resolution x-ray diffraction study

J. E. Boschker, C. Folkman, C. W. Bark, Å. F. Monsen, E. Folven, J. K. Grepstad, E. Wahlström, C. B. Eom, and T. Tybell

Phys. Rev. B **84**, 205418 — Published 14 November 2011

DOI: [10.1103/PhysRevB.84.205418](https://doi.org/10.1103/PhysRevB.84.205418)

Structural coupling across the LaAlO₃/SrTiO₃ interface

J.E. Boschker¹, C. Folkman², C.W. Bark², Å.F. Monsen³, E. Folven¹, J.K.Grepstad¹, E. Wahlström³, C.B. Eom², and T. Tybell^{1,#}

¹ *Department of Electronics and Telecommunications, Norwegian University of Science and Technology, 7491 Trondheim, Norway*

² *Department of Materials Science and Engineering, University of Wisconsin-Madison, Madison, WI 53706, USA*

³ *Department of Physics, Norwegian University of Science and Technology, 7491 Trondheim, Norway*

Abstract

Here we demonstrate a structural interaction between LaAlO₃ thin films and SrTiO₃ substrates using high resolution x-ray diffraction. X-ray diffraction profiles reveal the presence of periodic lattice distortions in the LaAlO₃ thin films, whose in-plane periodicity is determined by the miscut angle and miscut direction of the substrate. We show that the structural distortions in LaAlO₃ thin films induce similar distortions in the SrTiO₃ substrate.

Corresponding author: (e-mail) thomas.tybell@iet.ntnu.no

Heteroepitaxy is a powerful method to enhance and control the properties of functional perovskite materials.^{1,2} The physical ground state is closely related to the local symmetry of the perovskites. By controlling the oxygen octahedra rotations, physical deposition offers the possibility to tune the electronic properties of perovskite thin films, as observed for LaNiO₃ thin films.³ Moreover, at an interface between two perovskites with different symmetry, a structural coupling across the interface is possible. For example the interfacial coupling of oxygen octahedral rotations in PbTiO₃/SrTiO₃ superlattices can stabilize improper ferroelectricity,⁴ allowing for the coexistence of magnetism and a strong magneto-electric coupling.⁵

Recently the 2-dimensional electron gas (2DEG) at the LaAlO₃/SrTiO₃ interface has attracted large attention,⁶ resulting in the observation of magnetic effects⁷ and superconductivity⁸ at the interface and possible device applications have been demonstrated.^{9, 10} There is a symmetry difference between the SrTiO₃ and LaAlO₃,¹¹ opening for the possibility of structural coupling across the interface. The crystal structure of LaAlO₃ is rhombohedral at room temperature, however commonly described as pseudocubic with a lattice constant of 3.79 Å and a lattice angle of 90.087°, which is due to the rotations of the oxygen octahedra¹² (the subscripts pc and c will be used to differentiate between the pseudocubic and cubic symmetry). Epitaxial LaAlO₃ below the critical thickness of 3.8 nm has been reported to be fully commensurate with the cubic SrTiO₃ substrate,¹³ and the LaAlO₃ lattice adjusts its in-plane lattice parameter to the in-plane lattice parameter of SrTiO₃, which is 3.905 Å.¹⁴ Transmission electron microscopy has revealed that the rotation of the oxygen octahedra in LaAlO₃ couple to the oxygen octahedra in SrTiO₃ and induce oxygen octahedra rotations in the three SrTiO₃ unit cells adjacent to the interface.¹⁵

However, a complete understanding of the conductance of this interface and the influence of defects, such as oxygen vacancies and intermixing, is still lacking.¹⁶⁻¹⁹ Recent experiments revealed that the interface conductance decreased with increased LaAlO₃ layer thickness²⁰ and that the electron mobility decreased toward the interface.²¹ Furthermore, anisotropic electrical transport dependent on the step and terrace structure of the substrate, has been observed.²² An effect of the lower symmetry of LaAlO₃ with respect to SrTiO₃ is the possibility of ferroelastic domain formation that can affect the transport properties of the interface, for example in La_{0.9}Sr_{0.1}MnO₃ thin films the formation of periodic in-plane lattice modulations²³ disturb the conductance of such films.

The low symmetry and the lattice misfit of LaAlO₃ thin films with respect to the SrTiO₃ substrate must be considered in order to understand the LaAlO₃/SrTiO₃ interface structure. Here, we use LaAlO₃ thin films on (001)_c SrTiO₃ as a model system to study the structural interaction between films and substrates with a symmetry mismatch. Using x-ray diffraction (XRD), we observe lattice distortions in LaAlO₃ thin films whose periodicity is correlated with the step-and-terrace surface of the substrates. We demonstrate that the lattice distortions in the LaAlO₃ film couple through the interface and induce corresponding lattice distortions in the SrTiO₃ substrate. Furthermore, we show that this structural coupling gives rise to an interface crystal structure of SrTiO₃ which depends on the LaAlO₃ layer thickness.

LaAlO₃ thin films were grown on TiO₂ terminated (001)_c SrTiO₃ substrates by pulsed laser deposition using a single crystalline LaAlO₃ target at a distance of 4.5 cm from the substrate. For the deposition, a KrF excimer laser ($\lambda=248$ nm), with a repetition rate of 1 Hz and a fluency of ~ 2 J/cm², a substrate temperature of 650-750°C, and an oxygen ambient of 0.01-0.03 mbar was used. Prior to deposition, the substrates were annealed in oxygen for one hour at

950°C. After the deposition the samples were cooled at a rate of 15 °C/min in a 0.1 bar oxygen ambient. In situ reflection high-energy electron diffraction (RHEED) was consistent with layer-by-layer growth, and atomic force microscopy (AFM) showed that all the samples had a clear step and terrace structure. The crystalline quality was investigated with four circle XRD (D8, Bruker) equipped with a temperature dome (Anton Paar, DHS 900). The thin films used in this study were grown in thicknesses ranging from 8 to 19 nm in order to allow for large signal to noise ratio in the XRD studies. Fits of the Scherrer equation to the thickness fringes in θ - 2θ scans confirmed the film thicknesses, as inferred from the RHEED analysis. From the $(002)_{pc}$ reflection a typical out-of-plane lattice parameter of 3.78 Å was obtained. The typical full width at half maximum of the rocking curves for the $(001)_{pc}$ reflection of the films was $\sim 0.03^\circ$, compared to a value of $\sim 0.02^\circ$ for the substrates. Reciprocal space maps around SrTiO_3 $(103)_c$ reflection were made in order to ascertain the in-plane lattice constant. All films were close to coherent, and only showed a slightly relaxed in-plane lattice constant, as shown in Fig 1(a) and in agreement with Qiao *et al.*²⁴ We attribute the absence of a critical thickness for strain relaxation due to lattice mismatch to domain formation.²⁵

High resolution reciprocal space maps were recorded around the LaAlO_3 $(001)_{pc}$ reflection in order to study the crystal structure of the LaAlO_3 films in detail. Diffuse scattering satellite peaks can be seen in these reciprocal space maps, Fig. 1(b) displaying a set of representative data for a 19 nm thick LaAlO_3 film. Linear q_x scans around the $(001)_{pc}$ and $(002)_{pc}$ reflections, Fig. 1(c), show that the satellite peaks have a constant separation from the Bragg reflection in reciprocal space, which indicates that the satellite peaks derives from a periodic change of the crystal structure and not from twinning. Another possible cause for the observed satellite peaks are misfit dislocations.²⁶ An estimated of the periodicity of misfit

dislocations was determined using $a_{\text{LaO}}a_{\text{Sto}}/(a_{\text{Sto}}-a_{\text{LaO}})$, where a is the in-plane lattice constant. For the sample in Fig. 1(c), which has an in-plane lattice constant of $3.90\pm 0.02\text{\AA}$, an average periodicity of 300 nm was estimated for misfit dislocations. Since, the real space periodicity of the structural modulation is inversely proportional to the satellite to Bragg peak separation, Δq_x , it equals 166 nm for the sample in Fig 1(b) and is thus in disagreement with the estimated periodicity for misfit dislocations. No correlation between the observed relaxations and the in-plane periodicities was observed in this study. Furthermore, a decrease in the satellite intensity and a constant Δq_x were observed upon further relaxation upon high temperature annealing. Therefore, it is concluded that misfit dislocations do not explain the observed structural modulation.

The reciprocal space maps for the $\text{LaAlO}_3(001)_{\text{pc}}$ reflection, as shown in Fig 1(b), also revealed that the position of the satellite peaks was centered at a lower q_z value than the main Bragg reflection. The positions of the satellite peaks and the Bragg reflection were determined by fits using the Scherrer equation. The separation in q_z between the satellite peaks and the Bragg reflection was determined at $\Delta q_z = (4\pm 1)\cdot 10^{-4}\text{\AA}^{-1}$ for the film in Fig 1(b). It was found that Δq_z increases with the in-plane lattice constant, hence the degree of epitaxial coherency as shown in Fig. 1(d). Hence the data reveal no dependence on the film thickness. Furthermore, the position of the diffuse scattering surrounding the satellite peaks was also centered at a lower q_z value than the main Bragg reflection. The lower q_z values for the positions of the satellite peaks and the surrounding diffuse scattering are typical for an in-plane structural modulation with a periodic increase in the out-of-plane lattice constant.²⁶ The observed separation corresponds to an expansion of the out-of-plane lattice constant of $0.15\pm 0.04\%$. Hence there is an in-plane

structural modulation in the LaAlO₃ film due to periodic distortions with an increased larger out-of-plane lattice constant.

The surface topography of the LaAlO₃ films was studied in order to identify possible origins of the observed structural distortions. Figure 2(a) shows an AFM image of a 15 nm thick LaAlO₃ film. The only visible surface structure is the step-and-terrace structure due to the miscut of the substrate. From the AFM image an average terrace width of 250 nm and a miscut direction $\beta = 16 \pm 5^\circ$, defined as the angle between the [010]_c axis of the substrate and the projection of the surface normal on (001)_c plane, are obtained. In order to probe a possible influence of the step-and-terrace morphology on the observed structural distortions, linear q_x scans of the LaAlO₃ (001)_{pc} reflection were made at different azimuthal angles, φ , i.e. the angle between the in-plane direction probed by XRD and the [010]_c axis of the substrate, see Fig. 2(a). Figure 2(b) shows the observed Δq_x as a function of φ (red crosses). The structural modulation has a twofold symmetry, with a maximum at $\varphi = 15^\circ$, which equals the miscut direction of the substrate. Furthermore, the dashed line in Fig. 2(b) corresponds to $1/d$, the reciprocal width of the substrate terraces as a function of φ . The clear correlation testifies to the fact that the minimum in-plane periodicity in the LaAlO₃ film is the same as the width of the substrate terraces, and that the minimum periodicity is observed parallel to the miscut direction of the substrate. A similar correspondence was observed for all samples in this study having thicknesses between 8 and 19 nm. Figure 2(c) shows the minimum periodicity, as determined from the maximum satellite to Bragg peak separation, as a function of the terrace width of the substrate. This clear correlation shows that the in-plane periodicity is determined by the step-and-terrace structure of the substrate. An estimate of the length of the distortions perpendicular to the miscut direction can be obtained from the angular dependence. However, when Δq_x is

smaller than $2 \cdot 10^{-4} \text{ \AA}^{-1}$, the satellite peaks and the Bragg reflection start to overlap, and the satellite peaks cannot be resolved. The present study therefore places a lower limit on the maximum distortion length along the terraces at approximately 2 times the terrace width.

LaAlO₃ being rhombohedral can have up to four structural variances when deposited on cubic SrTiO₃. Ferroelastic domain walls can accommodate strain, as for example seen for BiFeO₃ thin films.²⁵ This is in agreement with the present data, the larger degree of coherency between the thin film and the substrate, see Fig. 1 (d), the larger the observed effect of periodic in-plane modulations. Such structural boundaries can form at the substrate step-edges during sample growth, and are in LaAlO₃ characterized by an absence of the rotation of the oxygen octahedra and a change in volume of the unit cell,²⁷ as illustrated in Fig 3(b). Twin walls are thus a possible cause for the observed structural modulation. In order to test this hypothesis, the thickness dependence of the satellite intensity, $I_{LaAlO_3}^{satellite}$, relative to that of the SrTiO₃ Bragg reflection, I_{SrTiO_3} , was examined. The x-ray data was compared with the calculated values using an

approximation:²⁸ $\frac{\overline{\Delta F_{LaAlO_3}}}{F_{SrTiO_3}} \approx \sqrt{\frac{I_{LaAlO_3}^{satellite}}{I_{SrTiO_3}^{Bragg}} \frac{\tau}{n}}$, τ being the x-ray penetration depth in SrTiO₃, n the

LaAlO₃ layer thickness and $\overline{\Delta F_{LaAlO_3}} / F_{SrTiO_3}$ the ratio between the structure factor of the periodic modulation in LaAlO₃ and the SrTiO₃ structure factor. Figure 3(a) shows that $\overline{\Delta F_{LaAlO_3}} / F_{SrTiO_3}$ increase with increasing film thickness, indicating that the observed modulation is a bulk effect. Furthermore, it shows that the LaAlO₃ satellite peak intensity, $I_{LaAlO_3}^{satellite}$, increases faster than the thickness squared, which would be expected from an increase in thickness alone. In order to understand this thickness dependence, an approximation of $\overline{\Delta F_{LaAlO_3}}$ was made. The approximation is based on the observed volume expansion of 0.15% at the structural boundaries

and the absence of oxygen octahedral rotations of 5° , which is the bulk value at room temperature,¹² as illustrated in Fig 3(b), and it is given by:

$$\overline{\Delta F_{lao}} \approx \frac{1}{m} \sum_1^m \sum_a f_a \left[e^{i2\pi q_z c z_{domain}^a} - e^{i2\pi q_z c (z_{domain_wall}^a + (m-1+z_{wall}^a)\Delta c/c)} \right],$$

where f_a is the atomic form factor of the different atoms in the unit cell, q_z the reciprocal lattice unit, c the out-of-plane lattice constant of LaAlO_3 , z^a the atomic position in the domain (wall), Δc the observed lattice expansion and m the number of unit cells in the LAO layer. Calculations of $\overline{\Delta F_{LaAlO_3}} / F_{SrTiO_3}$ revealed an increase in $\overline{\Delta F_{LaAlO_3}} / F_{SrTiO_3}$ with thickness, but failed to explain the observed trend, i.e. the blue line in Fig 3(a). Oxygen vacancies are likely to be present at structural boundaries,²⁹ and defects would result in a thickness independent contribution to $\overline{\Delta F_{LaAlO_3}} / F_{SrTiO_3}$. Including oxygen vacancies in the LaO plane in these calculations it was possible to fit the observed trend. The red dashed line is a fit based on the inclusion of oxygen vacancies. From this fit, the oxygen content of unit cells at the boundary was found to be 2.5 ± 0.1 . Fits using vacancies in the AlO_2 plane, or a combination of both planes which is more probable, rendered a higher vacancy concentration. These results give a lower limit for the oxygen content in the domain wall, because complimentary cation vacancies, having a more pronounced contribution to the scattered x-rays, also contribute to the satellite intensity. We note that the assumptions underlying the calculation of $\overline{\Delta F_{LaAlO_3}}$ can result in a scaling error. Therefore, the data was also fitted using an additional scaling factor. In this case, an improved fit was also obtained by including vacancies in the calculation.

Although structural distortions have been observed in epitaxial perovskite thin films, the interaction of such distortions with the substrate is less studied. In order to investigate a possible coupling between the distortions in LaAlO_3 and the SrTiO_3 substrate, linear q_x scans of the

SrTiO₃ substrate were made along the [010]_c direction on the (101)_c, (001)_c and (002)_c reflections before (dashed lines) and after (solid lines) the deposition of the LaAlO₃ films. As shown in Fig. 4(a), no satellite peaks were observed before the deposition, which confirms that the observed distortions discussed above originate in the LaAlO₃ layer. However, all three reflections showed satellite peaks with an identical separation in reciprocal space after the deposition. Reciprocal space scans revealed a clear separation in q_z for the satellites to the LaAlO₃ and SrTiO₃ Bragg reflections, respectively. Thus, in agreement with that the satellites to the SrTiO₃ reflection do not originate from LaAlO₃ reflections. Moreover, in Fig 2(b) the measured Δq_x for SrTiO₃ (blue circles) and LaAlO₃ (red crosses) are compared as a function of the azimuth angle, φ . These observations are clear evidence that the lattice distortions in the SrTiO₃ substrate are caused by the distortions in the LaAlO₃ thin film. A possible cause for the observed structural coupling could be a compression of the SrTiO₃ lattice due to the expansion of the LaAlO₃ lattice. This would suggest a higher q_z value for the SrTiO₃ satellite peaks. However, the width and intensity of the SrTiO₃ Bragg reflection prevents observation of this separation. We note that 38 nm thick La_{0.7}Sr_{0.3}MnO₃ thin films grown on SrTiO₃ substrates also exhibit similar step-edge induced structural modulations. However, the effect is less pronounced as evidenced by a lower satellite to Bragg intensity ratio and no measurable separation of the satellites from the Bragg reflection in q_z . Furthermore, it was not possible to observe a coupling from La_{0.7}Sr_{0.3}MnO₃ to SrTiO₃. This indicates that coupling into the substrate depends on the degree of distortion at the structural boundary as compared to domains of the thin films.

In Fig 3 it was shown that the structure factor difference of the LaAlO₃ films increases with increasing film thickness. In order to study how this affects the distortions in SrTiO₃, the substrate satellite peaks were examined as a function of the LaAlO₃ film thickness. It is expected

that the distortions are present only near the interface. Therefore, an exponential decay of the structure factor difference is introduced, as illustrated in Fig 4(b). The integrated intensity of the SrTiO₃ satellites, $I_{SrTiO_3}^{satellite}$, is thus proportional to $\frac{\lambda}{2} \left| \overline{\Delta F_{SrTiO_3}} \right|^2$, where $\left| \overline{\Delta F_{SrTiO_3}} \right|$ is the structure factor difference between the distortions in SrTiO₃ and the undistorted SrTiO₃, and λ is the penetration depth of the distortions into the substrate. The integrated satellite intensity was determined by fitting the linear q_x scans of the (001) reflection to Voigt functions, and by multiplying the obtained area with the FWHM in q_z . Figure 4(c) shows that $\sqrt{I_{SrTiO_3}^{satellite}}$, normalized to the maximum value, exhibits a near linear increase with the LaAlO₃ film thickness and becomes constant above approximately 15 nm. Since $\sqrt{I_{SrTiO_3}^{satellite}}$ is proportional to $\left| \overline{\Delta F_{SrTiO_3}} \right|$, $\left| \overline{\Delta F_{SrTiO_3}} \right|$ exhibits a similar dependence on LaAlO₃ film thickness as $\overline{\Delta F_{LaAlO_3}}$. The linear increase can be explained in terms of a quadratic increase of the penetration depth with LaAlO₃ film thickness, a linear increase of the structure factor difference in SrTiO₃ with LaAlO₃ film thickness or a combination of these. From the present data it is not possible to distinguish between these scenarios. However we note that the structure factor difference for LaAlO₃ increased closely to linearly with LaAlO₃ thickness.

In order to determine the penetration depth of this structural distortion, it is assumed that λ is constant, and that the ratio of the satellite peaks with respect to the Bragg reflection is the same for SrTiO₃ as for LaAlO₃. Based on these assumptions, an average λ of 50±20 nm was determined. Assuming a larger distortion in SrTiO₃, a reduced penetration depth would be obtained. This estimate thus services as an upper bound of the penetration depth. Nevertheless, it is clear that the penetration will affect the electron gas at the LaAlO₃/SrTiO₃ interface, which extends approximately 4 nm into SrTiO₃ at room temperature.³⁰ We therefore expect that the

observed distortions in SrTiO₃, which increase with the LaAlO₃ film thickness, will lower the conductivity of the LaAlO₃/SrTiO₃ interface in the LaAlO₃ film thickness range investigated.³¹ Furthermore, a linear fit of the thickness dependent data below 15 nm, see Fig 4(c), suggests that thinner LaAlO₃ films will also induce distortions in the SrTiO₃ substrate. Bell *et al.* indeed observed a decrease in conductivity with increasing film thickness [15]. Nevertheless, more detailed studies are needed to clarify the implications of the observed distortions on the conductance at the LaAlO₃/SrTiO₃ interface.

In conclusion, our results show that the step-and-terrace structure of SrTiO₃ substrates can give rise to ordering of lattice distortions in LaAlO₃ thin films. It was demonstrated that the observed lattice distortions induce corresponding lattice distortions in the SrTiO₃ substrate. These results not only show that the crystal structure of a thin film depends on the substrate, but also show that the crystal structure of the upper atomic layers of the substrate is affected by the growth of a low symmetry thin film. These results are important for all devices based on perovskite materials having a lower symmetry than the substrate, and for devices based on the interface conductivity in particular since similar distortions in the blanket of thin films affects their conductivity.

This project was supported by the Norwegian Research Council under project number 10239707. The work at University of Wisconsin-Madison was supported by the National Science Foundation under Grant No. DMR-0906443 and a David and Lucile Packard Fellowship (C.B.E.).

References

- 1 K. J. Choi, et al., *Science* **306**, 1005 (2004).
- 2 J. H. Haeni, et al., *Nature* **430**, 758 (2004).
- 3 S. J. May, J. W. Kim, J. M. Rondinelli, E. Karapetrova, N. A. Spaldin, A. Bhattacharya,
and P. J. Ryan, *Physical Review B* **82**, 014110 (2010).
- 4 E. Bousquet, M. Dawber, N. Stucki, C. Lichtensteiger, P. Hermet, S. Gariglio, J. M.
Triscone, and P. Ghosez, *Nature* **452**, 732 (2008).
- 5 N. A. Benedek and C. J. Fennie, *Physical Review Letters* **106**, 107204 (2011).
- 6 A. Ohtomo and H. Y. Hwang, *Nature* **427**, 423 (2004).
- 7 A. Brinkman, et al., *Nature Materials* **6**, 493 (2007).
- 8 N. Reyren, et al., *Science* **317**, 1196 (2007).
- 9 S. Thiel, G. Hammerl, A. Schmehl, C. W. Schneider, and J. Mannhart, *Science* **313**, 1942
(2006).
- 10 C. Cen, S. Thiel, J. Mannhart, and J. Levy, *Science* **323**, 1026 (2009).
- 11 D. L. Proffit, H. W. Jang, S. Lee, C. T. Nelson, X. Q. Pan, M. S. Rzchowski, and C. B.
Eom, *Applied Physics Letters* **93**, 111912 (2008).
- 12 S. A. Hayward, et al., *Physical Review B* **72**, 054110 (2005).
- 13 C. Merckling, M. El-Kazzi, G. Delhaye, V. Favre-Nicolin, Y. Robach, M. Gendry, G.
Grenet, G. Saint-Girons, and G. Hollinger, *J. Cryst. Growth* **306**, 47 (2007).
- 14 D. deLigny and P. Richet, *Physical Review B* **53**, 3013 (1996).
- 15 C. L. Jia, S. B. Mi, M. Faley, U. Poppe, J. Schubert, and K. Urban, *Physical Review B*
79, 081405 (2009).
- 16 A. Kalabukhov, R. Gunnarsson, J. Borjesson, E. Olsson, T. Claeson, and D. Winkler,
Physical Review B **75**, 121404 (2007).
- 17 F. J. Wong, R. V. Chopdekar, and Y. Suzuki, *Physical Review B* **82**, 165413 (2010).
- 18 P. R. Willmott, et al., *Physical Review Letters* **99**, 155502 (2007).
- 19 M. Huijben, A. Brinkman, G. Koster, G. Rijnders, H. Hilgenkamp, and D. H. A. Blank,
Advanced Materials **21**, 1665 (2009).
- 20 C. Bell, S. Harashima, Y. Hikita, and H. Y. Hwang, *Applied Physics Letters* **94**, 222111
(2009).
- 21 C. Bell, S. Harashima, Y. Kozuka, M. Kim, B. G. Kim, Y. Hikita, and H. Y. Hwang,
Physical Review Letters **103**, 226802 (2009).
- 22 P. Brinks, W. Siemons, J. E. Kleibeuker, G. Koster, G. Rijnders, and M. Huijben,
Applied Physics Letters **98**, 242904 (2011).
- 23 U. Gebhardt, N. V. Kasper, A. Vigliante, P. Wochner, H. Dosch, F. S. Razavi, and H. U.
Habermeier, *Phys. Rev. Lett.* **98**, 096101 (2007).
- 24 L. Qiao, T. C. Droubay, T. Varga, M. E. Bowden, V. Shutthanandan, Z. Zhu, T. C.
Kaspar, and S. A. Chambers, *Physical Review B* **83**, 085408 (2011).
- 25 H. W. Jang, et al., *Advanced Materials* **21**, 817 (2009).
- 26 V. M. Kaganer, R. Kohler, M. Schmidbauer, R. Opitz, and B. Jenichen, *Physical Review*
B **55**, 1793 (1997).
- 27 W. T. Lee, E. K. H. Salje, and U. Bismayer, *Journal of Applied Physics* **93**, 9890 (2003).
- 28 M. Birkholz, *Thin Film analysis by X-Ray Scattering* (Wiley-VCH Verlag GmbH & Co.,
2006).
- 29 R. J. Harrison, S. A. T. Redfern, and E. K. H. Salje, *Physical Review B* **69**, 144101
(2004).

30

M. Basletic, et al., Nature Materials 7, 621 (2008).

31

It was not possible to investigate thinner LaAlO₃ films due to the limited intensity of the XRD setup.

Figure Captions

FIG. 1 (color online) (a) The in-plane lattice constant, a , as a function of film thickness. (b) Reciprocal space map around the LaAlO_3 $(001)_{\text{pc}}$ reflection of a 19 nm thick LaAlO_3 film on (001) SrTiO_3 . (c) X-ray diffraction linear q_x scans of LaAlO_3 $(001)_{\text{pc}}$ reflection (red (lower) line) and $(002)_{\text{pc}}$ reflection (blue (upper) line). Similar data was obtained for all thicknesses investigated in this study. (d) The separation in q_z between the satellite and Bragg peaks as a function of in-plane lattice constant for as grown (circles).

FIG. 2 (color online) (a) AFM image of a 15 nm thick LaAlO_3 film with low-index the crystalline axes, the miscut direction, β , and the azimuth angle, φ , depicted. The miscut direction is $16 \pm 5^\circ$, and the terrace width is 250 nm. (b) The satellite separation, Δq_x , as a function of in-plane orientation, φ , for LaAlO_3 (red crosses) and SrTiO_3 (blue circles), and $1/d$, the reciprocal width of the terrace width, shown as a function of φ (dashed line). (c) The minimum periodicity as observed by XRD as a function of the substrate terrace width (blue squares), the line indicates where the modulation width is equal to the substrate terrace width.

FIG. 3 (color online) (a) The thickness dependence of the ratio between the averaged LaAlO_3 structure factor difference and the SrTiO_3 structure factor, $\overline{\Delta F_{\text{LaAlO}_3}} / F_{\text{SrTiO}_3}$ (red squares) [21] and calculated values for $\overline{\Delta F_{\text{LaAlO}_3}} / F_{\text{SrTiO}_3}$ with oxygen vacancies (dashed red (upper) line) and without oxygen vacancies (dashed blue (lower) line). (b) Illustration of the crystal structure in the domain and domain wall.

FIG. 4 (color online) (a) Linear q_x scans of the $(101)_c$ (magenta (lower) line), $(001)_c$ (blue (middle) line) and $(002)_c$ (red (upper) line) reflections of the SrTiO_3 substrate after (solid lines) and before (dashed lines) the deposition of a 15 nm thick LaAlO_3 film. (b) Illustration of the assumed depth dependence of the distortions in SrTiO_3 induced by distortions in the LaAlO_3 film. (c) The square root of the SrTiO_3 satellite intensity, $\sqrt{I_{\text{SrTiO}_3}^{\text{satellite}}}$, as a function of the LaAlO_3 layer thickness with a linear fit to the data below 15 nm.

Figure 1

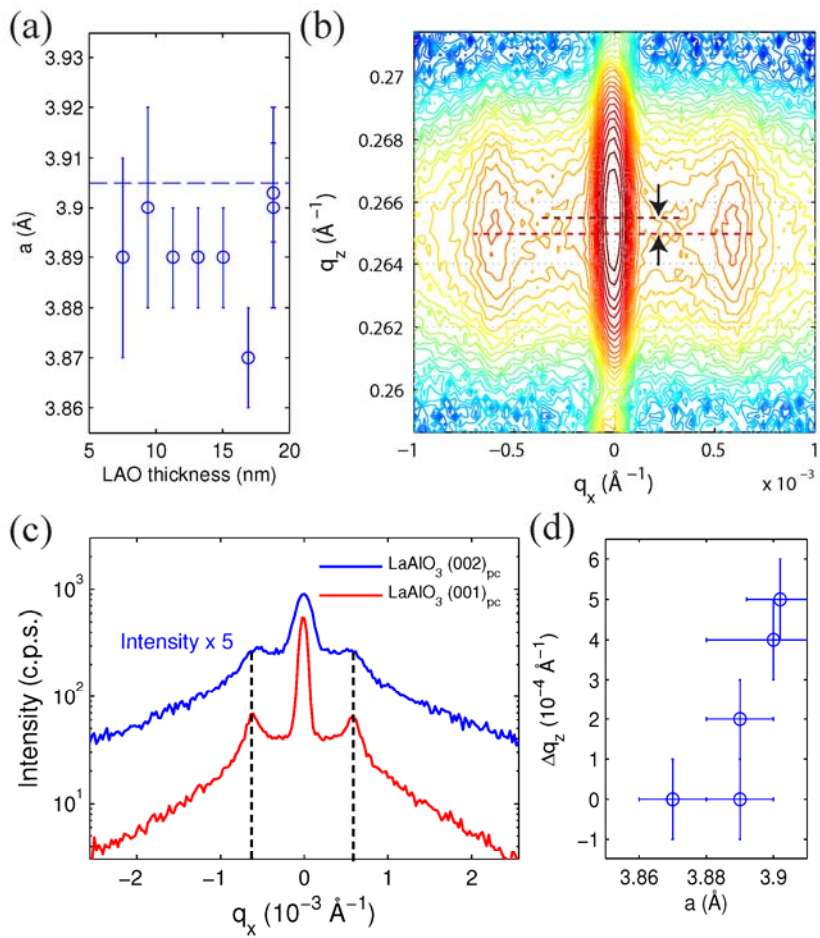


Figure 2

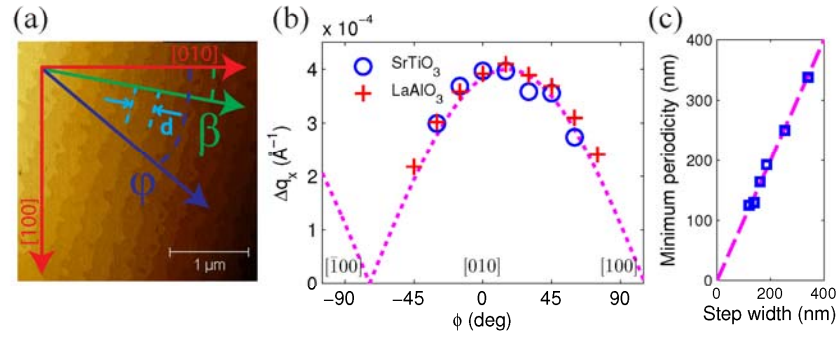


Figure 3

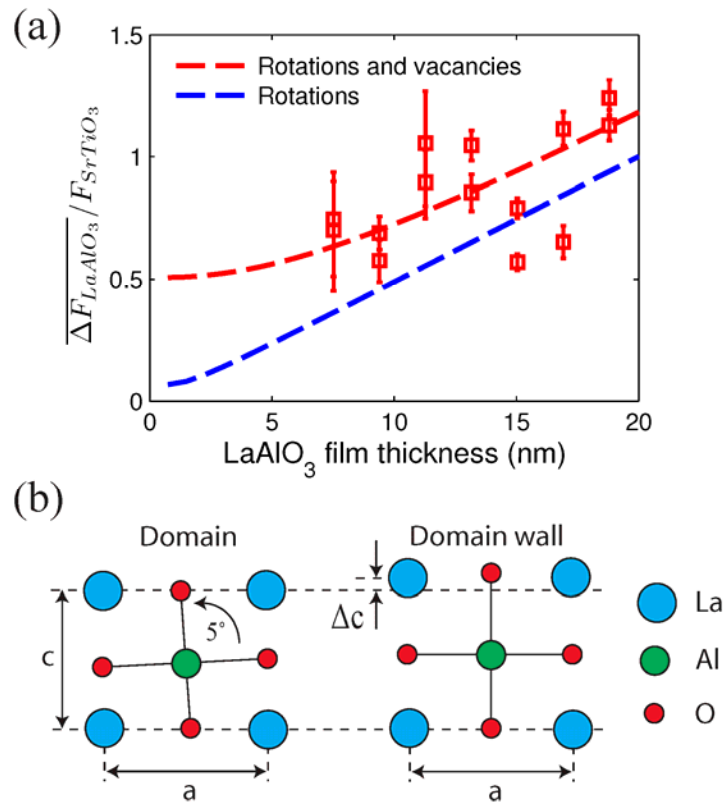


Figure 4

